NBSIR 85-3209

Radiation Measurements on A Portable 1.5 MEV Electron Linac

C.E. Dick, D. Polansky, C.G. Soares, and S.M. Seltzer

September 1985

NBSIR 85-3209

RADIATION MEASUREMENTS ON A PORTABLE 1.5 MEV ELECTRON LINAC

C.E. Dick, D. Polansky, C.G. Soares, and S.M. Seltzer

September 1985

Radiation Measurements on a Portable 1.5-MeV Electron Linac

C.E. Dick, D. Polansky, C.G. Soares, and S.M.Seltzer
Center for Radiation Research
National Bureau of Standards
Gaithersburg, MD. 20899

April 30, 1985

ABSTRACT

We have carried out an exhaustive series of measurements on the
properties of a 1.5 MeV electron linac designed for radiographic
applications. Measurements of the focal spot size, central axis
radiation intensity, radiation field uniformity, beam penetra-
tion, and radiation leakage have been made to characterize the
source. Additionally, Monte Carlo calculations of the source
output have been made to determine if the geometry is amenable to
a theoretical analysis. Although these data pertain to a
particular radiation source, the techniques described are
applicable to the characterization of a large class of radiation
producing devices.

1. INTRODUCTION

This report details measurements made on the radiation characteristics of a 1.5 MeV-electron linac. The main purpose of this report is to outline the procedures used to characterize radiation sources for possible applications in high energy radiography. The accelerator we have used is a commercial unit manufactured by the Schonberg Radiation Corporation in Mountain View, California (Minac Model T-1500)[1,2] and is designed for use in portable radiographic applications. We have investigated the operation and the properties of the radiation field produced by this device. These measurements have been divided into a number of tasks designed to measure the pertinent parameters of this source including the radiation intensity, the focal spot size, the field uniformity, the beam quality, and the radiation leakage. Additionally, based on the physical characteristics of the electron beam and x-ray converter, Monte Carlo calculations of the x-ray spectrum have been carried out. In the sections that follow, each of these topics is discussed in detail.

The accelerator consists of four basic modules which can be disconnected for transport. These modules are the control console, the x-ray head, the rf modulator and circulator, and the power unit. The accelerator was installed in a radiation shielded vault for personnel shielding. The initial setup of the accelerator took two people approximately four hours. This time would undoubtedly be reduced as familiarity is gained with the instrument.

The x-ray head contains the electron source, x-ray target,

and rf accelerating structure. This unit is provided with a vacion vacuum pump to provide the necessary high vacuum, and electrostatic beam steerers to center the electron beam on the x-ray target. RF power for acceleration of the electrons is provided by the rf-modulator chassis which is connected to the x-ray head with a flexible rf-waveguide. After the instrument was assembled, the power supply and vacion pump were energized. After approximately 5 minutes, the vacuum indicator read less than 1 microamp indicating that a good vacuum was obtained, and the vacuum interlock light on the console indicated a good vacuum status (lamp lit).

Upon completion of the above installation, the accelerator was left powered (except for the high voltage) for the duration of the testing period. Initially, no measurements were made for 24 hours to ensure that the vacuum in the accelerator was well established. All measurements discussed below were made with the following settings to provide reproducibility: AC input power variac maximum clockwise (meter indicates approximately 125 volts); accelerator heater control set at 80 as recommended in manufacturers operation manual; beam steerers both minimum (counterclockwise) in REV position. These controls do deflect the beam as can be seen in measurements of the radiation output on the central axis, but the effect is less than 5% in output and it was deemed desirable to have a reproducible setting of these controls at the expense of slightly higher output. It was noticed that the output exhibited a systematic increase for the first few days of operation. This may be due to the effects of a higher vacuum or a cleaning up of the accelerator structure.

2. MEASUREMENT OF FOCAL SPOT SIZE

In order to measure the size of the electron beam on the x-ray target, the geometry of Figure 1 was employed. A 1 mW He-Ne laser was used to define the central axis of the accelerator. The laser was located approximately 5 meters from the x-ray target and was left in place for all of the measurements to define the central axis of the radiation field. Reflection of the laser beam from a mirror mounted on the x-ray target indicated that the laser was coincident with the central axis of the accelerator to at least 0.1 degrees. A Pt-Au collimator with a thickness of 3 mm and containing a 300-μm hole was placed 0.5 meter from the x-ray target. The pinhole was aligned on the axis using the laser beam. A shielded x-ray film cassette was placed at a distance of 1 meter from the x-ray source. This geometry provides unit magnification of the image of the focal spot.

The film cassette contained a 125-μm thick lead front screen, Kodak type M industrial radiographic film[1], and a 250-μm thick lead back screen to record the image of the pinhole. Images of the pinhole were made on the film for times of 4, 8, and 12 minutes at the full output of the accelerator. Visual measurements of the focal spot image with a measuring magnifier indicates that the focal spot is nearly round with a diameter of approximately 3 mm.

In order to verify this measurement, the radiograph was placed in a scanning microdensitometer and the film scanned in two orthogonal directions. The results of these scans are shown in Fig. 2. These data indicate that the size of the focal spot

Figure 1.   Schematic drawing of the geometry used for the
measurement of the electron focal spot on the x-ray target. The
dotted center line represents the beam from a He-Ne laser located
5 meters from the target. This geometry is typical of that used
for all of the measurements on the accelerator with the laser beam
being used to define the beam axis.

Focal Spot Geometry

Film Cassette

Lead Shielding

Pt–Au Collimator

X–Ray Collimator

Electron Beam →

0.5 meter

0.5 meter
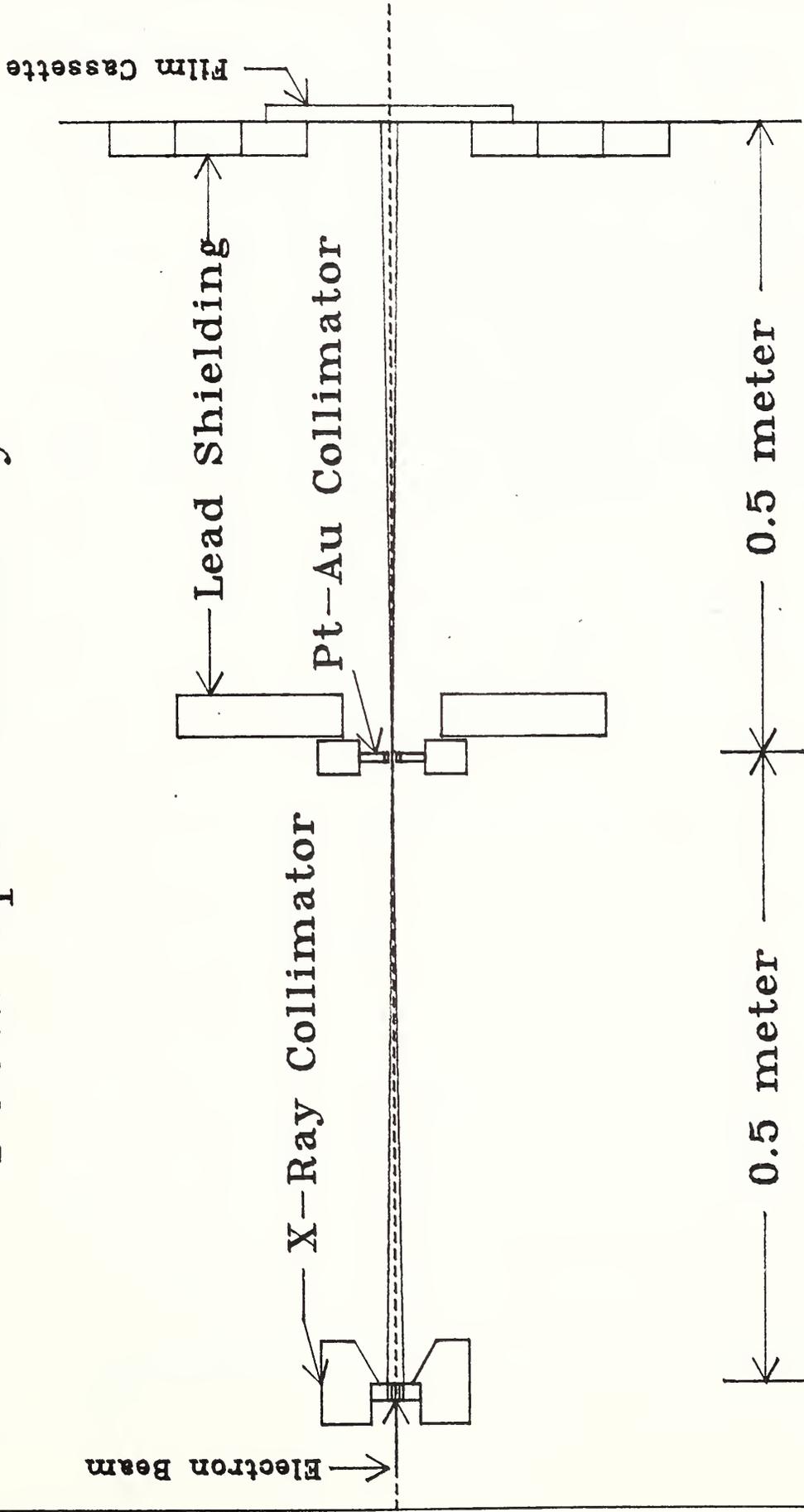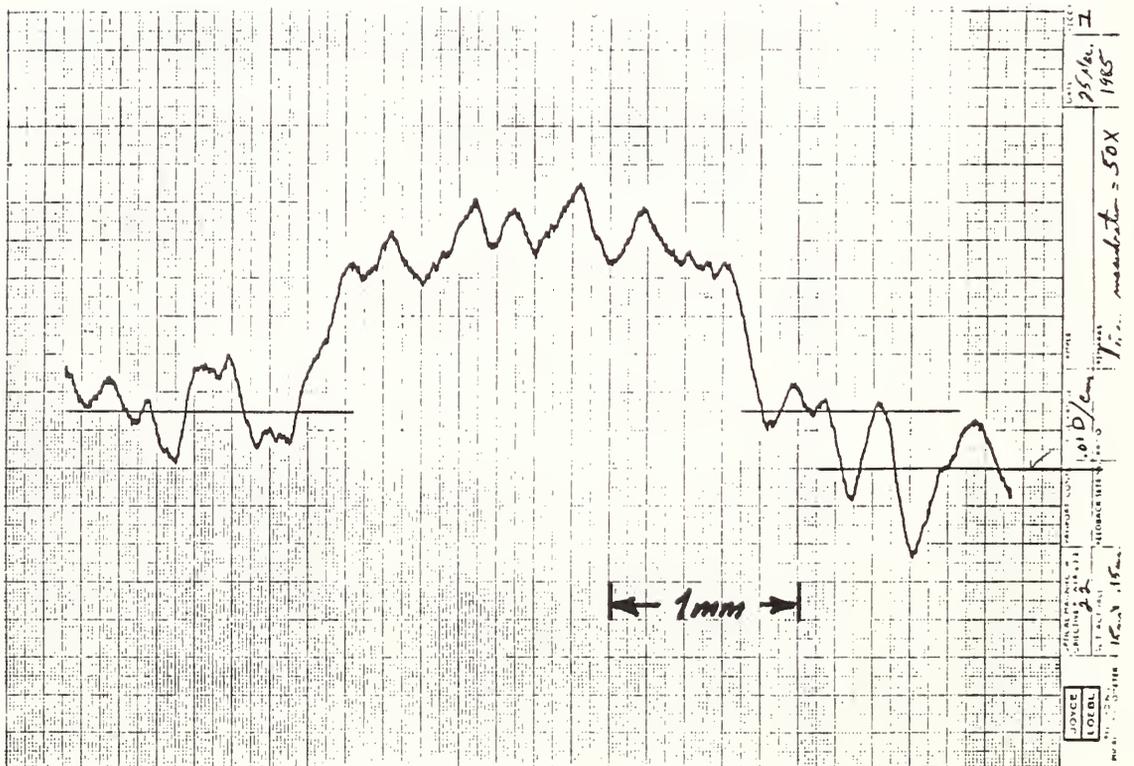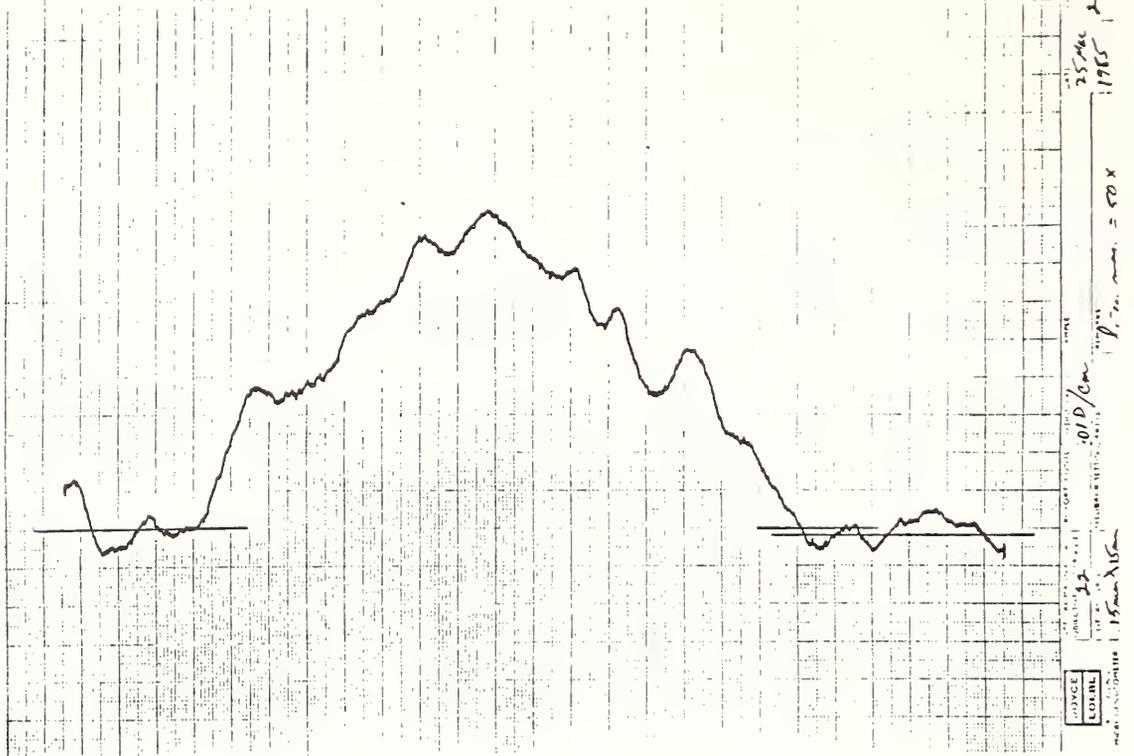
Figure 2. Microdensitometer traces of the image of the focal spot on the x-ray film. The magnification is a factor of 50, i.e. one large division is equivalent to 0.2 mm. in the horizontal direction. In the vertical direction, one division corresponds to .01 density units. The horizontal lines represent the base fog density.

(measured from the baseline fog level) is approximately
2.8 x 3.1mm. As a further check, the measurement was repeated
with a 125-μm pinhole in a 1.25 cm thick lead collimator
placed at the same location as the Pt-Au pinhole assembly. The
results of these measurements agree with the previous results to
within 5%.

3. THE CENTRAL AXIS RADIATION INTENSITY

In order to measure the radiation intensity on the central
axis of the accelerator, a Capintec Model 192 exposure meter[1] was
placed on the central axis with the aid of the laser at a distance
of approximately 1 meter from the x-ray target. This instrument
which uses a 0.5-cc ionization chamber and a lucite buildup cap was
calibrated in a standard ^{60}Co beam. The outside diameter of the
chamber is approximately 5 mm. In order to check the
effectiveness of the buildup cap, measurements were made with the
standard cap (17-mm diameter Lucite) and with other caps up to 60
mm diameter. The results of these measurements are given in
Table 1.

These data illustrate that the standard cap provides the
maximum buildup for the radiation field; this cap was used for
all the measurements with this chamber. Following these
measurements, the ionization chamber was positioned 1±0.05 meter
from the x-ray target. This measurement indicated that the
exposure rate at this location was 1.16±0.02 R/min. As indicated
earlier, measurements on successive days indicated that the
maximum exposure rate gradually increased from 1.16 to 1.35 R/min.
The accelerator is provided with a photosensitive diode mounted

next to the x-ray target to provide a relative measure of the radiation output. The readings on the current meter connected to this monitor were between 75 and 85 microamps for the outputs measured with the ionization chamber.

The readings obtained with the Capintec chamber were verified with an MDH ionization chamber (MDH Model 10X5-6)[1] with a 2 cm diameter bakelite buildup cap. The MDH reading agreed with the Capintec reading to within 2% for distances from 0.5 to 2 meters from the x-ray target.

As a final check, the radiation field intensity was checked for inverse-square-law dependence at distances from 0.5 to 3 meters from the source. The results of these measurements are given in Table 2. These data indicate that the source very closely follows the inverse-square-law dependence for a point radiation source with an intensity of approximately 1.2 to 1.3 R/min at 1 meter.

Table 1. Radiation intensity (R/min at ~1 meter) as measured with the Capintec ionization chamber and various Lucite buildup caps.

Buildup cap		
Diam. (mm)	Thickness(mm)	Exposure Rate (R/min)
17 (standard)	6	1.03
38	16.5	1.02
51	23	1.03
60	27.5	1.05

Table 2. Inverse-square-law check of the central-axis radiation intensity with Capintec chamber.

Source to chamber distance(meter)	Exposure Rate (R/min)	
	measured	calculated
0.5	4.61	4.64
1	1.16	assumed 1.16
2	0.27	0.29
3	0.12	0.13

4. THE BEAM INTENSITY PROFILE

In order to measure the beam intensity profile, the Capintec ionization chamber was mounted on an x-y positioner in a plane 1 meter from the x-ray target. This instrument is capable of remotely positioning the ionization chamber at any point up to 10.5 inches from the central position, both horizontally and vertically, with a reproducibility of 0.002 in. In order to normalize the measurements, a large MDH chamber (Model 10X5-180)[1] was centered on the beam axis approximately 30 cm from the x-ray target. Measurements were made with the Capintec chamber with and without the MDH chamber in place, and these data indicate that the MDH chamber used in this transmission mode did not affect the radiation intensity more than $\pm 1\%$ either on or off the beam axis.

Using this setup, measurements of the beam intensity were taken at approximately 250 locations in this plane. These data are shown in Fig. 3 and Table 3. In Fig. 3 the exposure rate (R/min) is plotted as a function of the distance from the center of the plane. This plot indicates that the beam is nearly circular in cross section with an intensity that drops to approximately 50% of the beam axis intensity between 5 and 6 in. from the beam axis. Beyond 10 inches from the beam axis, the intensity levels out at a nearly constant background level of about 7% of the forward intensity. This is consistent with the area subtended by the 30° collimator which gives a useful field of 21 in. diameter at 1 meter. In Table 3, the data are tabulated according to the actual horizontal and vertical location where they were recorded. In this table, the axis are drawn as they would be seen looking antiparallel to the x-ray

Figure 3. The exposure rate in a plane 1 meter from the x-ray target is plotted as a function of the distance from the beam axis. These data were measured with a 0.5-cc. ionization chamber and a remote x-y positioner described in the text.
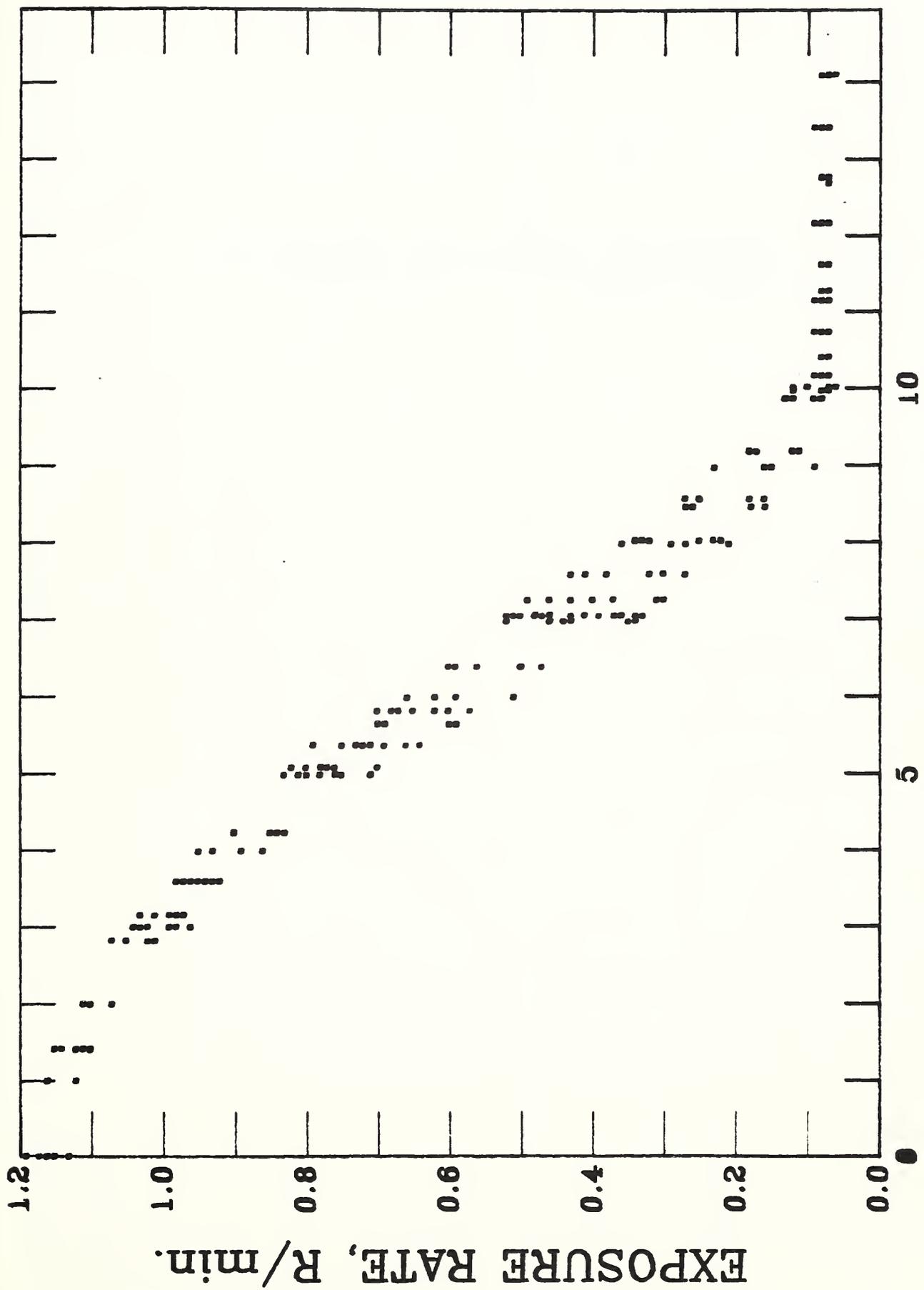
DISTANCE FROM CENTER, in.

EXPOSURE RATE, R/min.

Table 3. The exposure rates plotted in Fig. 3 are tabulated
according to the position in the plane where they were measured.
The values given are in R/min.

V \ H	-10	-9	-8	-7	-6	-5	-4	-3	-2	-1	H0	+1	+2	+3	+4	+5	+6	+7	+8	+9	+10
+10	0.08	0.07	0.07	0.07	0.07	0.07	0.07	0.07	0.07	0.06	0.07	0.07	0.07	0.07	0.07	0.07	0.08	0.08	0.07	0.08	0.07
+9	0.08	0.07									0.09									0.07	0.07
+8	0.08										0.21										0.07
+7	0.09			0.08							0.35							0.09			0.08
+6				0.12							0.51					0.16		0.12			
+5				0.18		0.38					0.71					0.37		0.18			
+4				0.25		0.50					0.86					0.50		0.23			
+3				0.32		0.60					0.97					0.62		0.30			
+2				0.40		0.69					1.07					0.71		0.37			
+1				0.43		0.76					1.12					0.78		0.41			
V0	0.07	0.15	0.29	0.46	0.62	0.78	0.93	1.04	1.11	1.16	1.16	1.16	1.11	1.01	0.89	0.78	0.59	0.44	0.27	0.16	0.08
-1				0.47		0.77					1.16					0.76		0.43			
-2				0.43		0.73					1.16					0.72		0.40			
-3				0.38		0.65					1.10					0.67		0.38			
-4				0.33		0.56					1.04					0.60		0.32			
-5				0.25		0.47					0.95					0.49		0.25			
-6				0.18		0.25					0.82					0.27		0.18			
-7				0.12							0.66					0.18		0.13			
-8											0.52										
-9	0.08										0.36										
-10	0.07										0.23										

beam. These data indicate that the beam is pointed slightly down and to the right as seen from the slightly higher readings in the lower right quadrant of the table. This slight asymmetry could be compensated by a different setting of the beam steering deflection coils at the end of the accelerator. All of the data presented in the table were normalized utilizing the MDH chamber as a transmission monitor.

5. THE X-RAY BEAM ENERGY

In order to measure the average x-ray energy, several techniques were used. In the first method, step wedges fabricated from cold-rolled steel were placed in front of a cassette containing a 125-μm thick lead front screen, Kodak Type T x-ray film[1], and a 250-μm thick back screen. The wedges are 2-in. wide by 8-in. high and have 4 steps on each wedge. These wedges were placed so as to be centered about the beam axis at a distance of 2 meters from the x-ray target. This distance was chosen to minimize the effects of the beam nonuniformity measured at 1 meter. The two step wedges have steps of 1/8-, 2/8-, 3/8-, and 4/8-in. and 0.5-, 1.0-, 1.5-, and 2.0-in., respectively. In order to monitor the exposure, the Capintec and small MDH chambers were placed in contact with the rear of the cassette on either side of the step wedges. Exposures of 0.5, 1.0, 2.0, 4.0, and 8.0 Roentgen were made in this geometry.

After exposure, the films were processed, and the optical density was measured in the center of each step with a densitometer. The resulting data are shown in Fig. 4. From these data, the half-value layer in steel was determined at optical

densities of 3, 2, and 1 density units (the horizontal lines in
Fig. 4). The solid lines in Fig. 4 are a computer generated
quadratic fit to the data of the form:

$$OD = at^2 + bt + c, \qquad (1)$$

where t is the steel thickness in inches. Table 4 presents the
values of these coefficients for the curves of Fig. 4. From these
parameters the half-value layers were calculated as 0.73-, 0.64-,
and 0.64-in of steel as shown by the vertical lines of Fig. 4.

Table 4. Coefficients for quadratic fit of step-wedge exposure
data of Fig. 4.

Curve Label	a	b	c
0.5 R	0.0566	−0.2714	0.4929
1.0 R	0.1501	−0.6093	0.8594
2.0 R	0.3235	−1.3851	1.8172
4.0 R	0.7165	−3.0673	3.8283
8.0 R	1.6344	−6.8519	8.2883

A second method was employed to measure the half-value layer
without the use of film. In this method, the Capintec small-
volume ionization chamber was placed approximately 1 meter from
the x-ray target and 0.5 in. to one side of the beam axis. The
small MDH chamber was placed 0.5 in. to the other side of the
beam axis and approximately 2 in. farther from the x-ray target.
Blocks of steel, brass, and aluminum measuring 2X2 in were placed
between the two chambers and the Capintec chamber reading was
used to normalize the MDH reading. Fig. 5 shows the results of

Figure 4. The optical densities measured from the images of a
steel step wedge are plotted as a function of the step thickness
for exposures from 0.5 to 8 R. The vertical dotted lines
represent the half-value layers determined from these data as
described in the text.

Type T Film

Lead Screens:
0.005" FRONT
0.010" BACK

8R
4R
2R
1R
0.5R

Optical Density
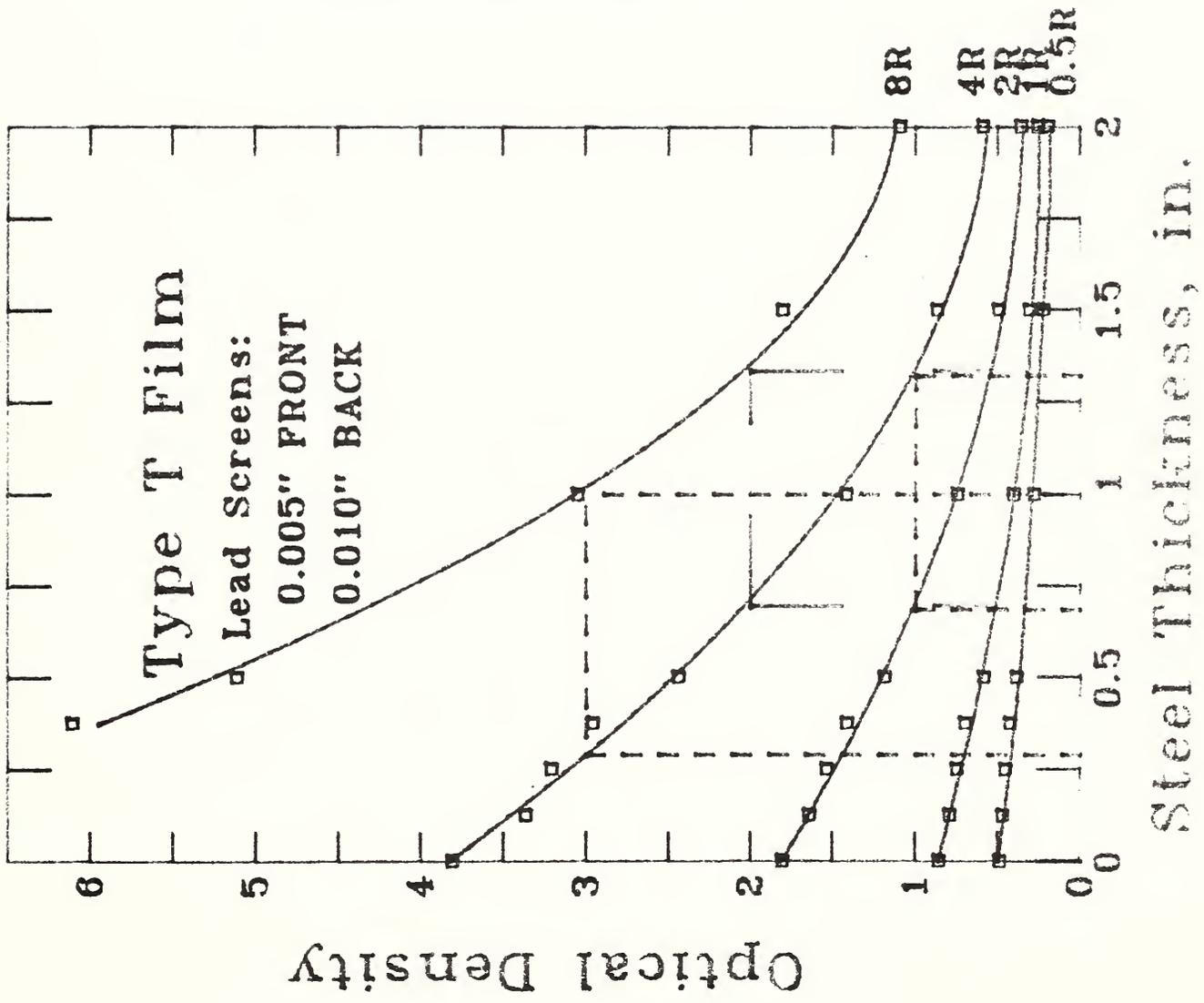
Steel Thickness, in.

Figure 5. The exposure rates measured with a 0.5-cc ionization chamber behind step wedges of aluminum, brass, and steel are plotted as a function of the step thickness. The table gives the values of the coefficients used for the quadratic fit of the data shown by the solid lines. The horizontal dotted lines indicate 1/2 and 1/4 of the primary intensity respectively.
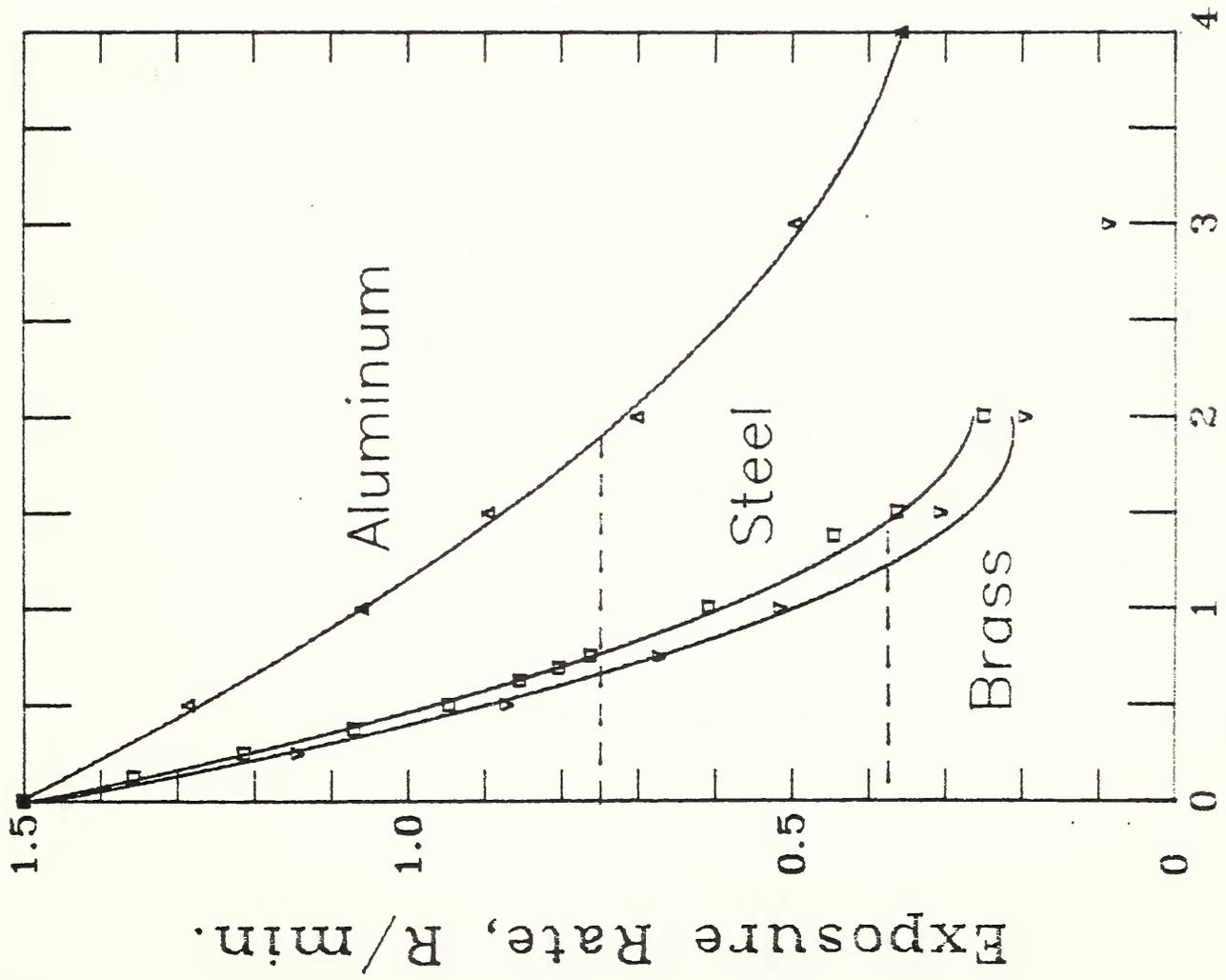
Fit of Form:

$y = ax^2 + bx + c$

Mat'l.	a	b	c
Brass	+0.341	−1.311	+1.470
Steel	+0.280	−1.172	+1.485
Alum.	+0.053	−0.499	+1.508

Aluminum

Steel

Brass

Material Thickness, in.

Exposure Rate, R/min.

this measurement and gives the values of the coefficients
generated to fit the data as before. From these data, it is
possible to calculate both the first and second half-value
thicknesses for these materials (the thickness of material
required to reduce the exposure to one-half and one quarter).
Table 5 gives these values for the three materials used.

Table 5. The first and second half-value thicknesses for the
Minac x-ray beam in various materials.

Material	Half-value thicknesses (in.)	
	1st	2nd
Aluminum	1.9	1.9
Brass	0.68	0.56
Steel	0.77	0.69

These data are consistent with the values for steel as
measured using the film technique described above and indicate
that in steel the equilibrium half-value thickness is
approximately 0.67 inches. This value corresponds to an
effective x-ray energy of approximately 1 MeV.[4]

In order to determine the energy of the electron beam
striking the x-ray target, an effort was made to measure the end
point of the bremsstrahlung spectra utilizing an ~60-cc high-
purity germanium detector. The detector was mounted in a lead
shield approximately 5 meters from the x-ray target and
approximately 10 degrees off the beam axis. In order to reduce
the counting rate in the detector, the accelerator was operated
at the lowest pulse rate and with the accelerator grid control

tuned for as low an output as possible. The beam was also
heavily filtered with approximately 15 cm of lead between the
source and the detector. The output of the detector was recorded
by a pulse height analyzer and the system was calibrated with
radioactive sources of ^{137}Cs and ^{60}Co. Due to the pulsed nature
of the radiation from the source, the measurement of the spectrum
was extremely difficult and time consuming. After a 2 hour run,
the data was extrapolated to determine the end point of the
spectrum. The results of this extrapolation indicate that the
electron energy is 1.43± 0.1 MeV. This value is reasonable
considering the effective energy of the photon beam of ~1 MeV
determined by the half-value measurements.

6. EXTENDED OPERATION

In order to test the long term operation of the accelerator,
it was operated continuously for a period of more than 8 hours.
The output of the accelerator was monitored with an ionization
chamber connected to an electrometer which was used to drive a
chart recorder. For the eight hour period, there were no
interruptions of the accelerator operation. For most of this
period, the accelerator was operated in the manual mode. Fig. 6
shows the output of the accelerator for several periods of time.
Fig. 6a illustrates the output for the first 30 minutes of
operation. This period is characterized by the need for periodic
retuning of the magnetron frequency to maintain maximum output.
The output for this period was approximately 1.3 R/min at 1 meter.
After approximately 45 minutes of running, the accelerator was
quite well stabilized and needed magnetron frequency adjustment

Figure 6. Chart recorder traces of the output of the accelerator during an extended run are shown. (a) First half-hour of operation; (b) Approximately 6 hours into run; and (c) After approximately 8.5 hours.

Long Term Stability Run
5-2-85

infrequently. Fig. 6b illustrates the operation approximately 6 hours into the run. The output is quite stable at approximately 1.22 R/min and there were no adjustments in the 20 min. period shown in this figure. Finally, Fig. 6c illustrates the operation near the end of the run and illustrates the effect of the AFC mode of operation. As can be seen from this figure, the AFC circuitry has the effect of detuning the magnetron and thus reducing the output. It may be that there is a fault in the feedback circuit used in this mode, but we made no attempt to troubleshoot this unit. However, the machine is stable enough in the manual mode so that it is quite usable for radiography.

7. X-RAY LEAKAGE

In order to measure the x-ray leakage outside of the primary beam, a 2-meter diameter ring was fabricated from 1/8 x 1/4 in. rectangular nylon stock. This ring was positioned in three orientations relative to the accelerator with the x-ray source at the center. These positions were: a) Parallel to the accelerator structure (horizontal); b) Perpendicular to the accelerator structure (vertical); and c) Slanted relative to the accelerator structure with the front end of the ring below the beam line at an angle of approximately 60° (slant). In order to measure the exposure, a series of thermoluminescent dosimeter (TLD) personnel badges were placed every 30° around the ring. Each badge contained four TLD's with various filters as follows: two lithium borate TLD's, one with no filter (#1) and one with a 300-mg/cm^2 plastic filter(#2); two calcium sulfate TLD's each with a 700-mg/cm^2 lead filter (#3 & #4). The badges were calibrated in a

standard ^{60}Co beam.

In order to normalize the TLD readings, the Capintec chamber was placed at 1 meter from the x-ray target on the beam axis. The TLD's were irradiated for an exposure on the Capintec of 10 R in each of the measurements. The data for each of the three cases (H,V, and S) are shown in the polar plots of Figs. 7-9 and given in Table 6. The data plotted in the figures is the data for TLD#2. For the horizontal data shown in Fig. 7, the maximum leakage is about 18% of the forward intensity and is at a maximum near 90°. The area behind the accelerator x-ray head is evidently shielded somewhat by the components in the structure itself. The large anomaly in the ratios of the TLD readings at 180° are indicative of a softening of the spectrum as would be expected at the large angles. Note that in the tabulated values the TLD's at 0° agree quite well with the integrated 10 R exposure measured by the ionization chamber. The vertical data of Fig. 8 indicate that the leakage in this plane is fairly uniform and about 18% of the forward intensity. The anamoly at 105° is not understood. Finally, the data at a slant of 60° indicate a similar behavior with a slightly higher leakage at the forward angles. These data indicate that the leakage around the accelerator is an appreciable fraction of the primary intensity and this necessitates that the operator of the instrument maintain a safe operating distance between the console location and the accelerator. A simple $1/r^2$ calculation indicates that for a forward intensity of 1 R/min at 1 meter the leakage at 60 meters from the source can be as high as 0.055 mR/min, with the minimum exposure rate being directly behind the accelerator.

Figures 7-9. Polar plots of the readings of TLD Element #2 as a percentage of the forward intensity, taken in horizontal (Fig. 7), vertical (Fig. 8), and slanted (Fig. 9) planes 1 meter from the x-ray target. The data were recorded at angular intervals of 30° as specified in the text.

Horizontal Plane

% of Forward Intensity

Vertical Plane

% of Forward Intensity

60° Slant Plane

% of Forward Intensity
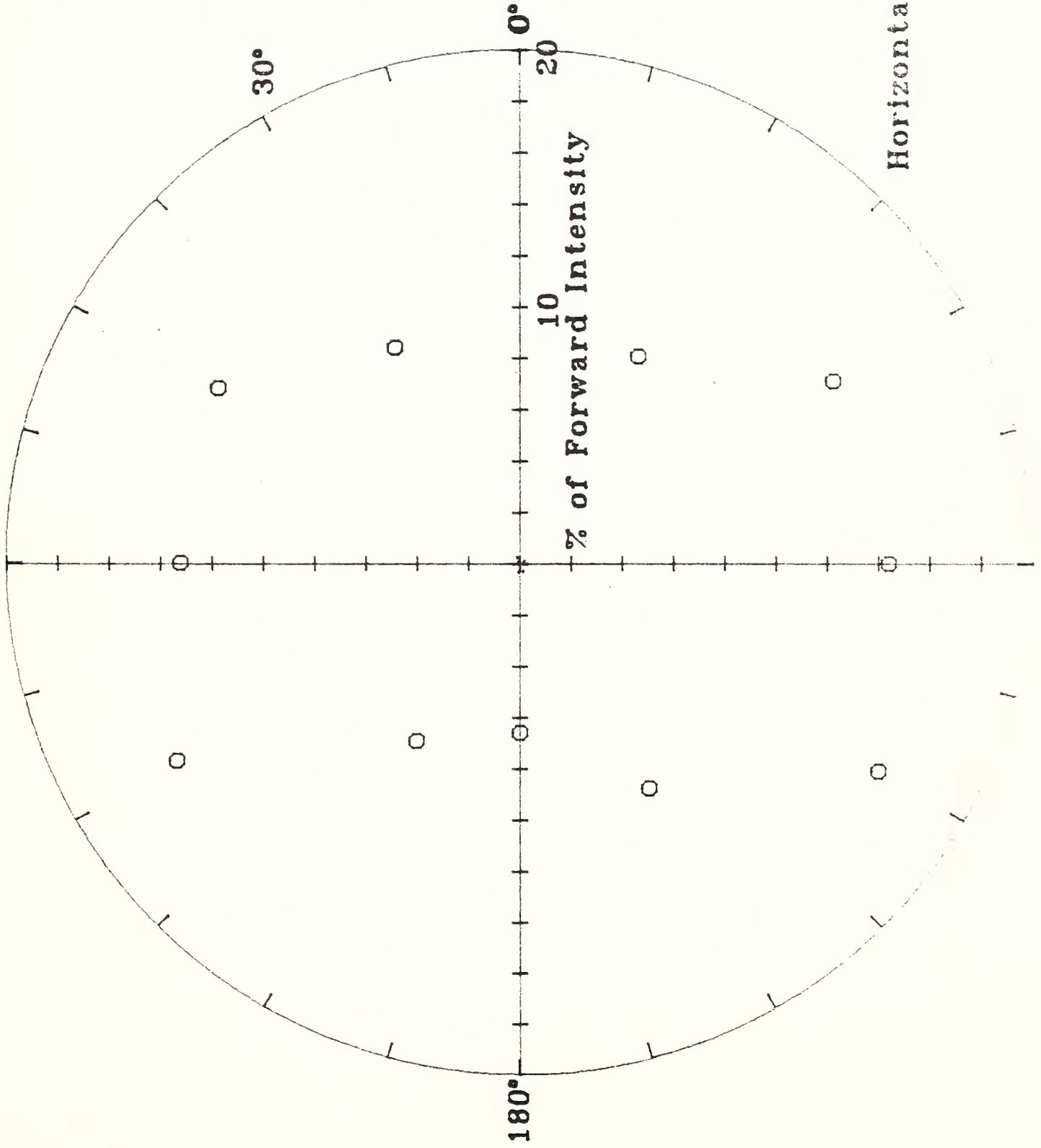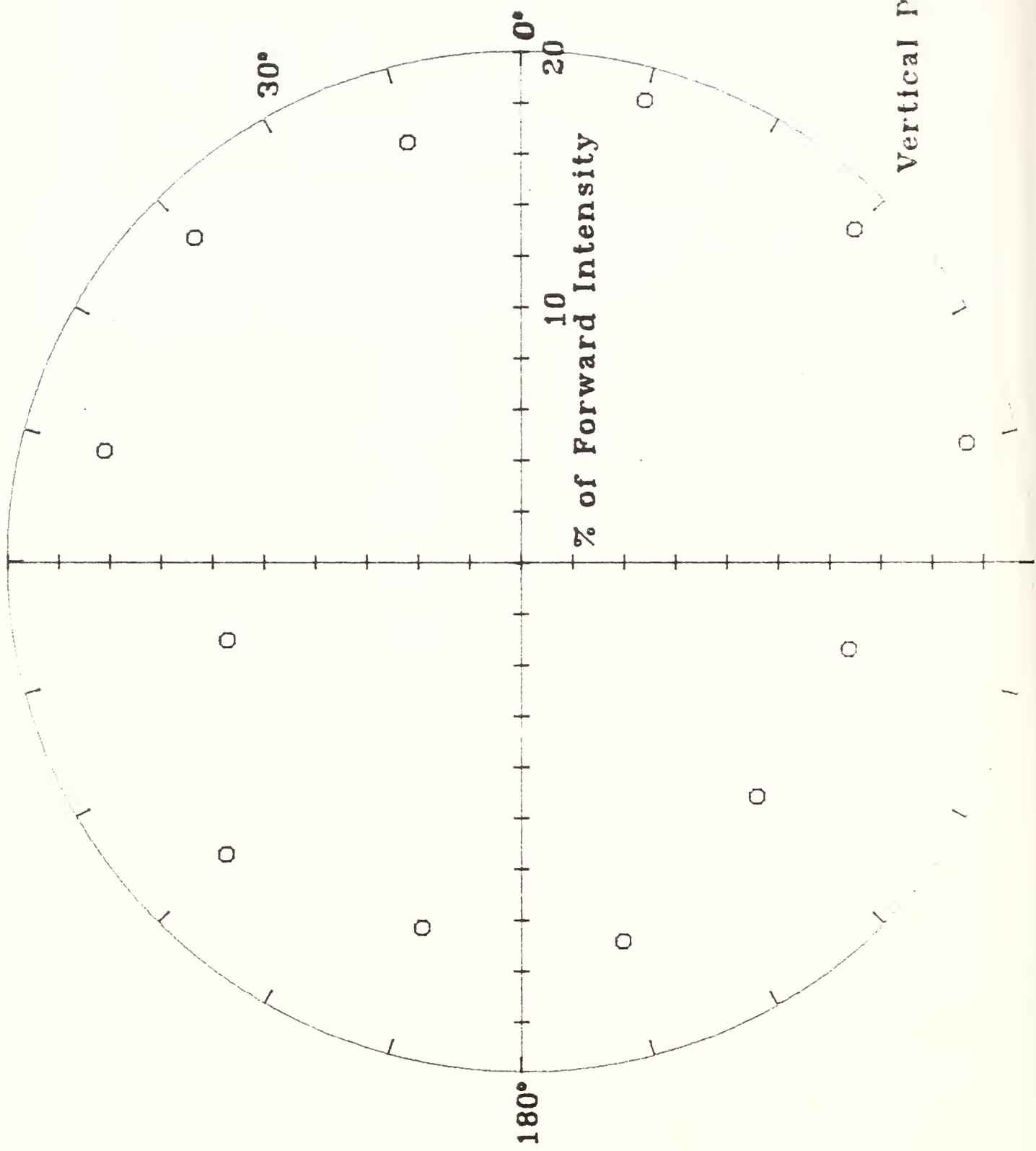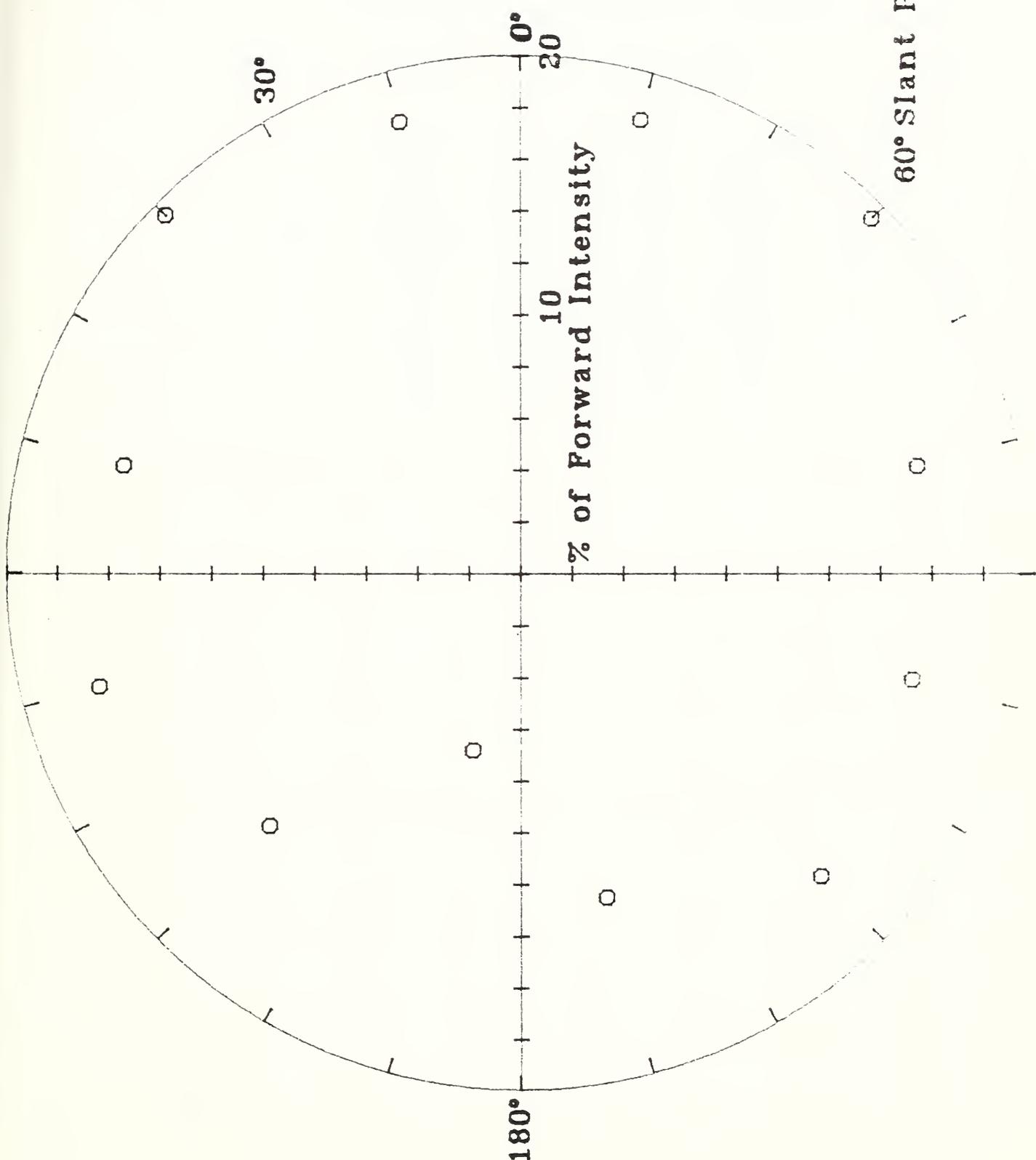
Table 6. Angular measurements of radiation leakage with TLD badges in horizontal, vertical, and slanted planes.

ANGLE Deg.	TLD#1	TLD#2 Values in mR	TLD#3	TLD#4	AVG. #3&#4	RATIOS #2/#3&#4	#3/#4
HORIZONTAL PLANE							
0	9417.7	9698.4	10196.8	9939.8	10058.9	0.963	1.026
30	1177.5	968.6	981.0	1000.2	990.5	0.978	0.981
60	1656.8	1354.6	1804.9	1796.8	1801.0	0.752	1.004
90	1511.3	1320.2	1832.1	1742.7	1789.8	0.739	1.051
120	1892.5	1542.4	1736.7	1654.0	1697.6	0.910	1.050
150	1607.7	801.1	1848.7	1809.3	1830.0	0.438	1.022
180	575.7	660.8	286.5	218.4	252.4	2.617	1.312
210	1166.3	1015.2	1063.0	1064.2	1063.6	0.955	0.999
240	1995.1	1619.7	2127.2	1709.5	1929.1	0.844	1.244
270	1801.8	1440.5	1900.3	1853.5	1878.1	0.767	1.025
300	1713.9	1412.9	1907.9	1898.5	1903.4	0.742	1.005
330	1253.1	927.4	965.3	982.8	974.0	0.952	0.982
VERTICAL PLANE							
15	2051.2	1699.2	2134.6	1733.8	1944.5	0.879	1.231
45	2010.4	1793.8	2094.3	2051.1	2073.7	0.865	1.021
75	2011.1	1675.1	1767.7	1688.2	1730.1	0.969	1.047
105	1403.2	1181.6	1232.5	1203.5	1218.1	0.970	1.024
135	1911.0	1623.9	1990.6	1942.6	1967.8	0.826	1.025
165	1893.0	1482.8	1754.1	1673.3	1715.9	0.865	1.048
195	1735.2	1537.0	2034.0	1996.6	2016.2	0.763	1.019
225	1637.7	1300.9	1845.2	1725.7	1788.6	0.729	1.069
255	1436.2	1320.9	1850.8	1467.8	1847.2	0.796	1.261
285	2069.4	1796.4	2124.6	2077.7	2102.3	0.855	1.023
315	2138.3	1836.9	2251.2	2220.5	2236.6	0.822	1.014
345	2104.9	1867.0	1869.6	1826.8	1849.3	1.010	1.023
60° SLANT PLANE							
15	2042.3	1801.2	2181.5	2109.9	2147.4	0.839	1.034
45	2380.4	1943.6	1954.4	2260.9	2100.3	0.922	0.864
75	1877.6	1592.8	2010.5	1935.9	1975.0	0.807	1.039
105	1880.4	1694.8	2049.8	2002.5	2027.3	0.836	1.024
135	1582.3	1381.1	1399.6	1378.0	1388.9	0.994	1.016
165	1060.5	709.2	782.9	707.1	745.2	0.952	1.107
195	1573.8	1298.0	1314.7	1320.1	1314.4	0.985	0.996
225	1923.0	1653.7	2102.3	2034.8	2070.1	0.799	1.033
255	2080.1	1579.1	2117.9	2032.1	2077.1	0.761	1.042
285	1918.0	1599.8	2027.9	1927.6	1980.2	0.890	1.052
315	2210.2	1932.5	1977.0	1936.8	1957.9	0.988	1.021
345	2056.3	1811.1	2147.7	2048.0	2100.2	0.863	1.049

8. CALCULATION OF THE X-RAY SPECTRUM

As indicated in Section 5, knowledge of the x-ray energy spectrum is largely inaccessible by direct measurement because of the well-known failure of most spectrometers to count in such a high-flux radiation field. In order to develop spectral information, Monte Carlo calculations were performed using the electron/photon transport code ZTRAN[5,6], a variant of the well-established Monte Carlo code ETRAN[7-12].

The Monte Carlo method treats in detail the complex process of bremsstrahlung production as the incident electrons slow down and change direction in the target, and the scattering and absorption of the emitted photons prior to escape from the target. Electron energy loss (including fluctuations), due to ionization and excitation events and due to bremsstrahlung emission, is accounted for throughout the electron histories; angular deflections from elastic and inelastic collisions are sampled along the electron trajectories. The photon histories are traced by sampling successive photon interactions in direct analogy to the physical process (Compton scattering, photoelectric absorption, and pair production).

The calculation takes into account all secondary radiations, including knock-on electrons from electron-impact ionization effects, bremsstrahlung and characteristic x rays, Compton electrons, photoelectrons, electron-positron pairs, and annihilation radiation. All generations of electrons and photons in the target with energies above chosen cut-off values are followed. A weighting scheme allows for the sampling of bremsstrahlung photon histories in excess of the natural

production rates so that statistical fluctuations in the bremsstrahlung results can be reduced without an increase in the time-consuming number of electron histories. The statistical accuracy of the photon results is also improved by scoring for each collision point in the photon history the probability that the photon crosses the boundaries of interest without further interaction (collision-density method).

The code makes use of a large body of electron and photon cross section data. The present calculations incorporate the latest information on electron stopping powers[13,14] and bremsstrahlung cross sections[15] and on photon interaction probabilities[16].

The distribution of emergent bremsstrahlung photons was calculated for 1.5-MeV electrons normally incident on a tungsten target 1.618 g/cm^2 (0.033 in.) thick and assumed to be laterally unbounded (semi-infinite slab). The tungsten layer was followed by a 0.1205 g/cm^2 thick air layer to account for the slight attenuation by 1 meter of air. The results are based on the simulation of 40,000 incident electron histories and of 1.2 million emitted bremsstrahlung photon histories. All generations of electrons and photons were followed until they escaped from the target or reached a cut-off energy of 100 keV.

Of interest in the present application is the fluence spectrum of photons transmitted in a small cone about the beam axis. The results indicate that there is only a small variation in the shape of the transmitted photon spectra with the angle of emergence. Therefore, the results integrated over emergent angles from 0 to 30 degrees to improve statistical accuracy are

used to represent the spectrum at 0°. The resultant energy-
weighted (intensity) spectrum ES(E) is shown in Fig. 10 and
tabulated in Table 7. The intensity spectrum has been
arbitrarily normalized to unit area (with energy in MeV). The
corresponding number spectrum S(E), obtained by dividing the
intensity spectrum in Fig. 10 or Table 7 by photon energy, has
an area of 2.05 with the present normalization.

Table 7. Energy-weighted intensity spectrum, ES(E) of x rays
transmitted by 0.033-in. W (+ 1 m air) bombarded by 1.5 MeV
electrons. Results are from Monte Carlo calculations.

Photon Energy E (MeV)	Intensity Spectrum ES(E)
0.100	0.000
0.125	0.078
0.150	0.269
0.175	0.490
0.200	0.758
0.250	1.180
0.300	1.298
0.350	1.343
0.400	1.328
0.450	1.270
0.500	1.201
0.550	1.129
0.600	1.058
0.700	0.913
0.800	0.785
0.900	0.672
1.000	0.572
1.100	0.482
1.200	0.390
1.300	0.296
1.400	0.129
1.500	0.000

In order to check the calculated x-ray spectrum against
measured quantities, the exposure from the calculated beam to a
small ionization chamber behind iron plates was estimated.
Considering only simple attenuation, the dose behind a iron slab

Figure 10. The calculated intensity spectrum ES(E) for the Minac
1500 linac. The corresponding number spectrum S(E) may be
obtained by dividing by the photon energy.
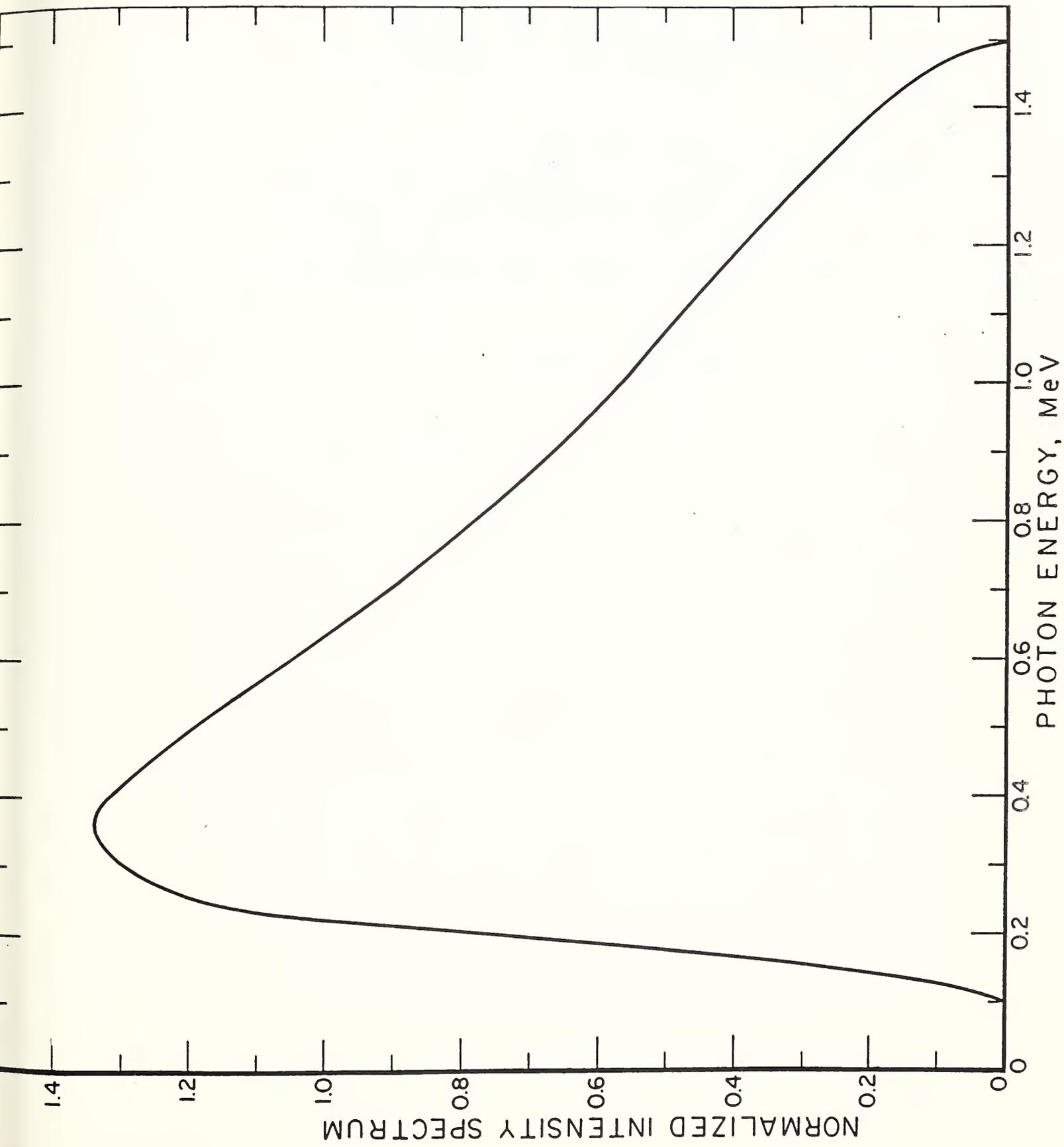
of thickness t is:

$$D_O(t) = \int dE \; E \; \mu_{en}^{air}(E) \; S(E) \; e^{-\mu(E)t}, \quad (2)$$

where $S(E)$ is the incident energy spectrum, $\mu_{en}^{air}(E)$ is the mass energy-absorption coefficient for air, and $\mu(E)$ is the narrow-beam attenuation coefficient for iron Eq. 2 ignores the contribution from photons scattered in the iron absorber, and therefore gives the dose to a point detector from an extremely thin pencil beam.

In order to include the dose from scattered photons, Monte Carlo calculations were done for the x-ray spectrum $S(E)$ normally incident on iron slabs with thicknesses $t = 13$, 20, and 40 g/cm^2. In each case the scattered photon fluence $F_S(E,t)$ in a small air volume was calculated for a broad beam, based on a sample of 0.5 million photon histories. The dose contributed by scattered photons is given by

$$D_S(t) = \int dE \; E \; \mu_{en}^{air}(E) \; F_S(E,t). \quad (3)$$

Table 8 gives the ratio $B(t) = D_S(t)/D_O(t)$, or the build-up factor so obtained.

Table 8. Dose build-up factors for transmission through iron slabs. Results pertain to a normally incident broad beam of photons with the calculated spectral distribution given in Table 7 and Fig. 11

Iron Thickness (g/cm^2):	0	13	20	40
Build-up factor:	0	0.739	1.08	2.06

Dose transmission curves are plotted in Fig. 11, based on $D_O(t)$ only (narrow beam) and on $D_O(t)$ plus $D_S(T)$ (broad beam). The

Figure 11. Calculated curves of dose transmission through iron plates, for narrow- and broad-beam geometries. The data points are the measured values from Section 6.
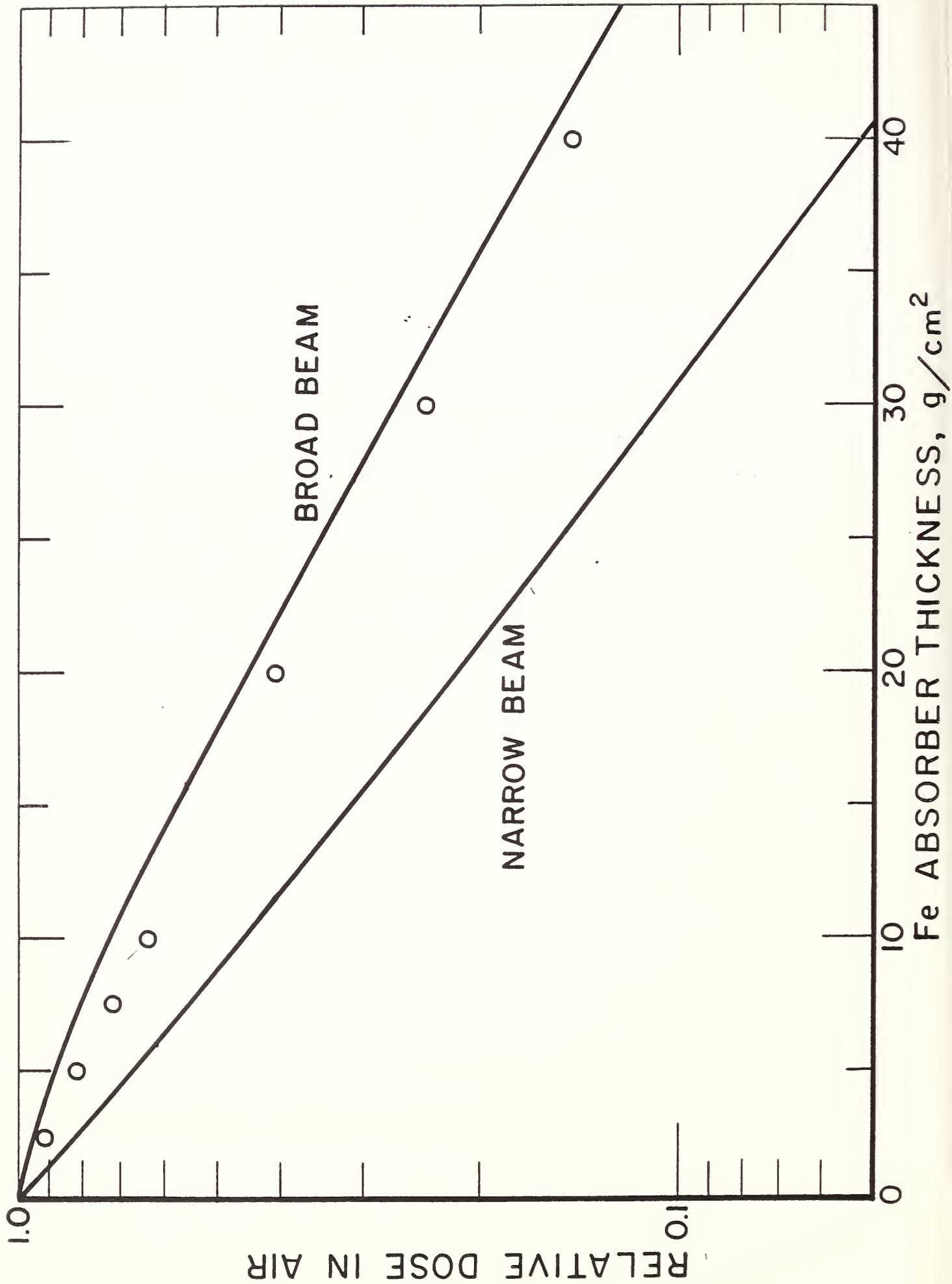
measured transmission data for the steel step wedges (Fig. 5) are plotted as points in Fig. 11. The actual measurement geometry is intermediate to narrow- and broad-beam conditions, being closer to broad beam geometry (with an effective beam radius corresponding to 1-3 mean free paths of the incident x rays). The first and second half-value thickness from the calculated results are compared to measured values in Table 9. The reasonably good agreement is sufficient to confirm consistency between calculated and measured results, and to obviate further photon transmission calculations in more complicated geometry.

Table 9. Comparison of measured and calculated half-value thickness for the Minac x-ray beam in steel plates.

| | Half-value Thickness (g/cm^2) | |
	Measured[a]	Calculated
1st	15.4	17.7
2nd	13.8	13.8

[a] Based on a density of 7.874 g/cm^3

---

10. TRIAL RADIOGRAPHS

In order to assess the usefulness of the linac for radiography, several trial radiographs were made. The first radiograph was of an electronic amplifier enclosed within a nuclear instrument module (NIM). This instrument is contained on one printed circuit board within a 1-in. thick module with 0.062 in. aluminum sides. The amplifier module was placed 2 meters from the x-ray target in contact with the x-ray film cassette. The film cassette was loaded with type T film and the same lead

intensifying screens used previously (125-μm front and 250-μm back). The small MDH ionization chamber was placed behind the amplifier, and the film was exposed for an integrated exposure of 2R.

Examination of the resulting radiograph shows the excellent detail that is present. The printed circuit traces consisting of 50-μm of silver on a 1-mm thick glass epoxy substrate are visible. Other objects with higher contrast such as the tantalum capacitors and the potentiometers are clearly imaged. In particular, the leads on a TO-5 transistor can are clearly visible as is the orientation tab.

In order to make an estimate of the detectability available, the steel step wedges used in the determination of the half-value layer were set up at the 2 meter location. A variety of penetrameters were placed in front of the step wedges, and a double-loaded film cassette was placed behind the assembly. The film cassette contained a 125-μm lead front screen, Kodak type M film, a 125-μm tantalum screen, Kodak type T film, and a 250-μm lead back screen. The penetrameters placed in front of the various steps of the steel wedge are listed in Table 10. In this table, the penetrameters labeled with the # sign are steel sheets with thicknesses in mils (1 mil = 0.001 in.) equal to the number of the penetrameter (i.e. #5 is 0.005 in. thick). In addition, each of these penetrameters has a 0.010-, 0.020-, and a 0.040 in. drilled hole. The penetrameters labeled 1-ISO-7 and 6-ISO-12 are wire penetrameters, each containing 7 steel wires. The 1-ISO-7 penetrameter has wires of 3.2-, 2.5-, 2.0-, 1.6-, 1.25-, 1.0-, and 0.8-mm diameter while for the 6-ISO-12 penetrameter,

the wire diameters are 1.0-, 0.8-, 0.63-, 0.5-, 0.4-, 0.32-, and 0.25-mm. The small MDH ionization chamber was centered behind the 1-and 1.5-inch steps, and the film was exposed until the MDH ionization chamber indicated a reading of 2R.

Table 10. Penetrameters placed in front of the steel step wedges.

Step Thickness (in.)	Penetrameter
0.125	Lead letters 'PEN' (no penetrameter)
0.250	#5 (0.005 in.) & #10 (0.010 in.)
0.375 & 0.500	1-ISO-7 wire penetrameter
0.500	#10 (0.010 in.) & #20 (0.020 in.)
1.000	#20 (0.020 in.)
1.500 & 2.000	6-ISO-12 wire penetrameter

After processing, the radiographs were visually inspected by a trained observer to determine the detectability of the various penetrameters. The results of these observations are given in Table 11 along with the optical densities measured behind each step of the wedges. The results of these observations indicate that there is a wide latitude of sensitivity available to the radiographer with the appropriate choice of x-ray film, and that 2% contrast differences (0.020 in./ 1 in.) can readily be detected.

Table 11. Detectability of various contrast differences from the penetrameter images tabulated in Table 10. The values in the table are the minimum sizes detectable. Percent values refer to the steel sheets, i.e. 2% in 2/8 in. indicates that the #5 penetrameter is visible on the 1/4 in. step.

t (in.)	[OD	M film Detectability	] [OD	T film Detectability	]
1/8	1.62		4.23		
2/8	1.56	2% contrast, .04" hole	4.05	2% contrast, .04" hole	
3/8	1.41	6 wires, .32 mm. dia.	3.63	7 wires, .25 mm. dia.	
4/8	1.25	5 wires, .40 mm. dia.	3.14	6 wires, .32 mm. dia.	
0.5	1.29	2% contrast, .02" hole	3.30	2% contrast, .02" hole	
1.0	0.85	2% contrast, .04" hole	2.01	2% contrast, .04" hole	
1.5	0.56	6 wires, 1.0 mm. dia.	1.18	7 wires, 0.8 mm. dia.	
2.0	0.39	5 wires, 1.25 mm. dia.	0.73	6 wires, 1.0 mm. dia.	

10. SUMMARY

We have outlined a series of measurements and calculations that were made to characterize a radiation source designed for radiographic applications. For this particular source, the pertinent parameters are summarized as follows:

- Focal Spot Size   3 mm.
- Half-value Layer   0.69 in. steel
- Electron Energy   1.5 MeV
- Off axis leakage   ~ 18 %
- Output   1.2 R/ min at 1 meter

From these data, a radiographer can select the operating parameters necessary for the completion of a particular radiographic task and utilize the source in a safe and efficient manner.

11. ACKNOWLEDGEMENTS

12. REFERENCES

1. Throughout this report certain commercial products are mentioned by name. This identification is for informational purposes only to specify experimental procedure. This does not imply that the products mentioned are necessarily the best or the only ones available for the purpose or imply endorsement by the National Bureau of Standards.

2. R.G. Schonberg, R.H. Miller, J.N. Weaver, W. Johnson, W.R. Fowkes, and H. Deruyter, Bull. Am. Phys. Soc. 30, 926 (1985).

3. Unless otherwise specified, all film was processed at 68 °F for 8 min. in Kodak GBX developer followed by 30 sec. in the stop bath and 8 min. in Kodak GBX fixer.

4. See for example; R. Halmshaw, The Physics of industrial Radiography, Elsevier Publishing Co., New York, (1966), pp 134-141.

5. S. M. Seltzer and M.J. Berger, NBSIR 84-2931 (1984).

6. S.M. Seltzer, J.P. Farrell, and J. Silverman, IEEE Trans. Nucl. Sci. NS-30, 1629 (1983).

7. M.J. Berger, Methods in Computational Physics (eds. B. Adler, S. Fernbach, and M. Rotenberg) Vol. 1, Academic Press, New York (1983).

8. M.J. Berger and S. M. Seltzer, NBS Reports 9836 and 9837 (1968); also available as Report CCC-107/ETRAN, Radiation Shielding Information Center, Oak Ridge National Laboratory.

9. M.J. Berger and S.M. Seltzer, Phys. Rev.C2, 621 (1970).

10. S.M. Seltzer, NBSIR 74-457 (1974).

11. S.M. Seltzer and M.J. Berger, Nucl. Instr. and Meth.119, 157 (1974).

12. S. M. Seltzer and M.J. Berger, NBSIR 78-1534 (1978).

13. S.M. Seltzer and M.J. Berger, Int. J. Appl. Radiat. Isot.33 1189 (1982); ibid. 33, 1219 (1982); ibid 35, 665 (1984).

14. M.J. Berger and S.M. Seltzer, NBSIR 82-2550-A (1983); M.J. Berger, H.H. Andersen, H. Bichsel, J.A. Dennis, M. Inokuti, D. Powers, S.M. Seltzer, and J.E. Turner, ICRU Report 37 (1984).

15. S.M. Seltzer and M.J. Berger, Nucl. Instr. Meth. B, in press; IEEE Trans. Nucl. Sci. NS-30, 4368 (1983).

16. J. H. Hubbell, Int. J. Appl. Radiat. Isot. <u>33</u>, 1269 (1982).

NBS-114A (REV. 2-80)

U.S. DEPT. OF COMM. BIBLIOGRAPHIC DATA SHEET (See instructions)	1. PUBLICATION OR REPORT NO. NBSIR 85-3209	2. Performing Organ. Report No.	3. Publication Date AUGUST 1985

4. TITLE AND SUBTITLE

Radiation Measurements on a Portable 1.5-MeV Electron Linac

5. AUTHOR(S)

C.E. Dick, D. Polansky, C.G. Soares and S.M. Seltzer

6. PERFORMING ORGANIZATION (If joint or other than NBS, see instructions) **NATIONAL BUREAU OF STANDARDS** **DEPARTMENT OF COMMERCE** **WASHINGTON, D.C. 20234**	7. Contract/Grant No.
	8. Type of Report & Period Covered

9. SPONSORING ORGANIZATION NAME AND COMPLETE ADDRESS (Street, City, State, ZIP)

10. SUPPLEMENTARY NOTES

☐ Document describes a computer program; SF-185, FIPS Software Summary, is attached.

11. ABSTRACT (A 200-word or less factual summary of most significant information. If document includes a significant bibliography or literature survey, mention it here)

We have carried out an exhaustive series of measurements on the properties of a 1.5 MeV electron linac designed for radiographic applications. Measurements of the focal spot size, central axis radiation intensity, radiation field uniformity, beam penetration, and radiation leakage have been made to characterize the source. Additionally, Monte Carlo calculations of the source output have been made to determine if the geometry is amenable to a theoretical analysis. Although these data pertain to a particular radiation source, the techniques described are applicable to the characterization of a large class of radiation producing devices.

12. KEY WORDS (Six to twelve entries; alphabetical order; capitalize only proper names; and separate key words by semicolons)

Electron linac, radiography, foral spot, radiation intensity, Monte Carlo calculations.

13. AVAILABILITY	14. NO. OF PRINTED PAGES
☒ Unlimited ☐ For Official Distribution. Do Not Release to NTIS ☐ Order From Superintendent of Documents, U.S. Government Printing Office, Washington, D.C. 20402.	50
☒ Order From National Technical Information Service (NTIS), Springfield, VA. 22161	15. Price $8.50